

# Hybrid magic state distillation for universal fault-tolerant quantum computation

Wenqiang Zheng,<sup>1,\*</sup> Yafei Yu,<sup>2,\*</sup> Jian Pan,<sup>1</sup> Jingfu Zhang,<sup>3</sup> Jun Li,<sup>1</sup> Zhaokai Li,<sup>1</sup> Dieter Suter,<sup>3</sup> Xianyi Zhou,<sup>1,†</sup> Xinhua Peng,<sup>1,4,‡</sup> and Jiangfeng Du<sup>1,4,§</sup>

<sup>1</sup>*Hefei National Laboratory for Physical Sciences at Microscale and Department of Modern Physics, University of Science and Technology of China, Hefei, Anhui 230026, China*

<sup>2</sup>*Laboratory of Nanophotonic Functional Materials and Devices,*

*LQIT & SIPSE, South China Normal University, Guangzhou 510006, China*

<sup>3</sup>*Fakultät Physik, Technische Universität Dortmund, 44221 Dortmund, Germany*

<sup>4</sup>*Synergetic Innovation Center of Quantum Information & Quantum Physics, University of Science and Technology of China, Hefei, Anhui 230026, China*

A set of stabilizer operations augmented by some special initial states known as “magic states”, gives the possibility of universal fault-tolerant quantum computation. However, magic state preparation inevitably involves nonideal operations that introduce noise. The most common method to eliminate the noise is magic state distillation (MSD) by stabilizer operations. Here we propose a hybrid MSD protocol by connecting a four-qubit *H*-type MSD with a five-qubit *T*-type MSD, in order to overcome some disadvantages of the previous MSD protocols. The hybrid MSD protocol further integrates distillable ranges of different existing MSD protocols and extends the *T*-type distillable range to the stabilizer octahedron edges. And it provides considerable improvement in qubit cost for almost all of the distillable range. Moreover, we experimentally demonstrate the four-qubit *H*-type MSD protocol using nuclear magnetic resonance technology, together with the previous five-qubit MSD experiment, to show the feasibility of the hybrid MSD protocol.

PACS numbers: 03.67.Lx, 03.67.Pp, 76.60.-k

Decoherence and control errors are some of the major obstacles for the implementation of scalable quantum information processing. To overcome these obstacles, quantum fault-tolerance theory has been developed [1, 2], in which the information is encoded in a subspace of a larger Hilbert space. The subspace is fixed by a subgroup of the Pauli group, consisting of some Hermitian tensor products of Pauli operators which are defined as the stabilizer of the subspace. Logical operations are *transversally* performed on the encoded information [3, 4], aiming to prevent the propagation of errors within the codeblock and further avoid correlated errors in the course of quantum error correction. Unfortunately, only a limited set of operations, known as *stabilizer operations* (consisting of Clifford group unitaries [5], preparation of  $|0\rangle$  and measurement in the computational basis), can be implemented in such a fault-tolerant manner, which can not provide a universal quantum computation according to the Gottesman-Knill theorem [6, 7]. This dilemma can be solved by introducing a nonstabilizer state (not eigenstates of Pauli operators) as an ancilla, and then implementing a gate outside the Clifford group through gate teleportation [1].

Preparation of a nonstabilizer state would inevitably involve non-stabilizer operations [8, 9], which are not fault-tolerant and induce noise to the nonstabilizer state. The most common method for reducing noise is to distill noisy copies of these resource nonstabilizer states to an almost pure nonstabilizer state with only stabilizer operations [8, 10, 11]. The pure nonstabilizer states that can be prepared through distillation with only stabilizer operations are called *magic states* and the fault-tolerant

distillation for magic states is called *magic-state distillation* (MSD). So far, there are two types of states found to be “magic”, and they are called *T*-type and *H*-type magic states [10]. Consequently, MSD enables universal fault-tolerant quantum computing, and it also opens a framework to observe what kind of quantum states can provide universal fault-tolerant computational power [12–14]. However MSD puts a big challenge to quantum computation as it will consume up a majority of qubit resource in architectures [15]. Much effort has been devoted to develop economical methods to get pure magic states by concatenating two MSD protocols of the same type magic state (*H*-type) [16], and to build up effective instructions to compile magic states and the stabilizer operations for implementing non-Clifford operations [17]. Besides, various MSD protocols suffer from different shortcomings. For example, for five-qubit *T*-type MSD [10] there is a gap between the distillable unstabilizer states and stabilizer states, for seven-qubit *H*-type MSD [11], the polarization of the output state increases only polynomially in the number of noisy copies at the range of high polarization, while four-qubit *H*-type MSD [18] cannot yield a nearly pure magic state.

Here we propose a novel MSD protocol by hybridizing one *H*-type MSD protocol [18] with one *T*-type MSD protocol [10]. This hybrid one does not only overcome the shortcomings in the previous MSD protocols mentioned above, but also brings two additional advantages: the integration of distillable ranges of previous individual MSD protocols and great reduction of qubit resource consumption. Moreover, up to now, the only experiment on the five-qubit *T*-type MSD has been implemented in nuclear

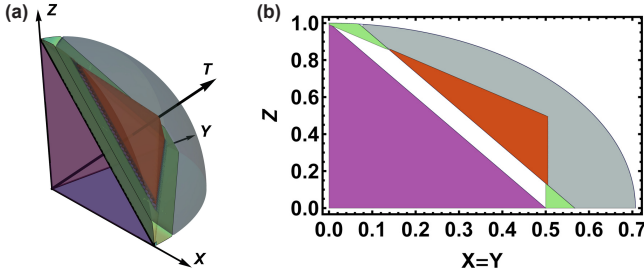


FIG. 1: Distillable ranges of the five-qubit  $T$ -type MSD protocol ( $\mathcal{A}_T$ , denoted as the gray and orange regions) and the seven-qubit  $H$ -type MSD protocol ( $\mathcal{A}_H$ , denoted as the green and orange regions). Purple region shows the interior of the stabilizer octahedron  $\mathcal{O}_s$ . (a) One octant of the Bloch sphere. (b) A cross-section of one octant of the Bloch sphere through the plane  $x = y$ .

magnetic resonance (NMR) system [19]. Here we report an experimental demonstration for the four-qubit MSD by NMR to show the feasibility of this hybrid protocol.

An arbitrary one-qubit state can be represented as  $\rho = (\mathbf{1} + x\sigma_x + y\sigma_y + z\sigma_z)/2$ , where  $\sigma_x, \sigma_y, \sigma_z$ , and  $\mathbf{1}$  denote the Pauli matrices and identity operator,  $\vec{a} = (x, y, z)$  is a dimensionless vector of length  $\leq 1$  that specifies the position of the state in the Bloch sphere. One single-qubit state  $\rho$  with  $|x| + |y| + |z| \leq 1$  (forming a stabilizer octahedron  $\mathcal{O}_s$ ) cannot be distilled to nonstabilizer states with only Clifford operations [20]. Prior MSD protocols show that some states outside  $\mathcal{O}_s$  can be distilled towards eigenstates of Clifford gates, such as the Hadamard  $H$  gate and the  $T$  gate [13, 21]. These eigenstates are magic states:  $H$ -type with  $\vec{a}_H = (0, \pm \frac{1}{\sqrt{2}}, \pm \frac{1}{\sqrt{2}}), (\pm \frac{1}{\sqrt{2}}, 0, \pm \frac{1}{\sqrt{2}}), (\pm \frac{1}{\sqrt{2}}, \pm \frac{1}{\sqrt{2}}, 0)$  and  $T$ -type with  $\vec{a}_T = (\pm \frac{1}{\sqrt{3}}, \pm \frac{1}{\sqrt{3}}, \pm \frac{1}{\sqrt{3}})$ . Without loss of generality, here we focus on two of them:

$$\begin{aligned} H\text{-type: } \rho_H &= [\mathbf{1} + (\sigma_x + \sigma_z)/\sqrt{2}]/2 \\ T\text{-type: } \rho_T &= [\mathbf{1} + (\sigma_x + \sigma_y + \sigma_z)/\sqrt{3}]/2. \end{aligned} \quad (1)$$

The polarization of an arbitrary state  $\rho$  in the direction of the magic states ( $H$ -direction or  $T$ -direction) is defined as

$$\begin{aligned} H\text{-type: } p_H(\rho) &= 2\text{Tr}(\rho \cdot \rho_H) - 1 = (x + z)/\sqrt{2} \\ T\text{-type: } p_T(\rho) &= 2\text{Tr}(\rho \cdot \rho_T) - 1 = (x + y + z)/\sqrt{3}, \end{aligned} \quad (2)$$

which quantifies how the state  $\rho$  is close to the magic states. Given a resource of these pure “magic” states, one can implement gates outside the Clifford group (i.e., the  $\pi/12$  phase gate for the  $H$ -type one and the  $\pi/8$  phase gate for the  $T$ -type one) to enable universal quantum computation.

Bravyi and Kitaev proposed a  $T$ -type MSD protocol based on five-qubit error correcting code [10]. Provided noisy copies have an initial polarization in  $T$ -direction

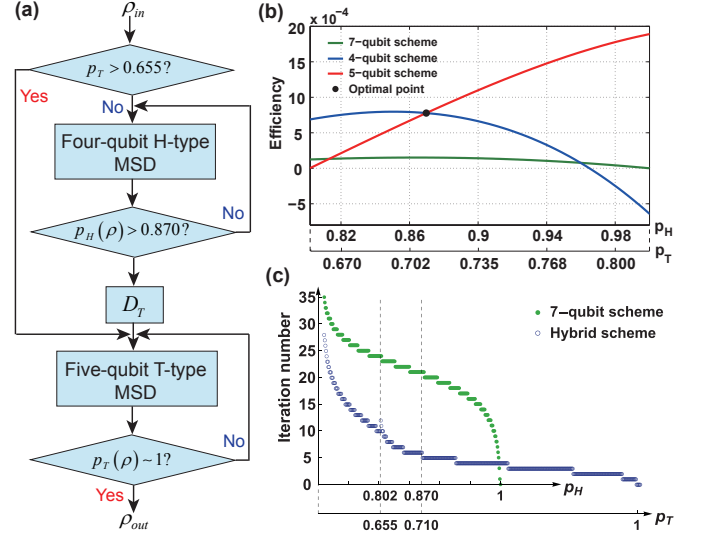


FIG. 2: (a) Flowchart of the hybrid MSD protocol  $D_T(\rho) = (\rho + T\rho T^\dagger + T^\dagger\rho T)/3$  is the  $T$ -projection operation. (b) The efficiency  $\nu$  of the MSD protocols for the state lying in  $H$ -direction. The second horizontal axis shows the corresponding  $p_T$ . The polarization loss resulted by  $D_T$  has been considered when we calculated the efficiency of the four-qubit protocol. (c) The necessary iteration number to distill noisy states for an almost pure magic state ( $T$ -type or  $H$ -type) with the target fidelity above 0.999.

$p_T(\rho_{\text{in}}) > \sqrt{3/7} \approx 0.655$ , this protocol yields a higher polarization. By the iteration, it is possible to obtain the output with  $p_T(\rho_{\text{out}}) \rightarrow 1$ . We define the distillable range by this  $T$ -type MSD protocol as  $\mathcal{A}_T$ , represented by the gray and orange regions in Fig. 1. There exhibits a gap between the region  $\mathcal{A}_T$  and the stabilizer octahedron  $\mathcal{O}_s$ . In contrast, Reichardt proposed a  $H$ -type MSD protocol based on the seven-qubit Steane code [11, 18]. It is possible to obtain the output with  $p_H(\rho_{\text{out}}) \rightarrow 1$  by this protocol, provided noisy copies have an initial polarization in  $H$ -direction  $p_H(\rho_{\text{in}}) > 1/\sqrt{2} \approx 0.707$ . We define this distillable range of the seven-qubit  $H$ -type MSD protocol as  $\mathcal{A}_H$ , represented by the green and orange regions in Fig. 1. The range  $\mathcal{A}_H$  is tight (no gap) in the directions crossing the octahedron edges, which means a transition from universal quantum computation to classical efficient simulation [13]. Alternatively, states can be distilled in the  $H$ -direction by using a four-qubit Clifford circuit [18], at the price of a smaller distillable range  $\mathcal{A}'_H \subset \mathcal{A}_H$ , where the ultimate polarization  $p_H(\rho_{\text{out}})$  is approximately equal to 0.964, not 1. From Fig. 1, we can see that the distillable ranges of the  $H$ -type and  $T$ -type MSD protocols do not overlap completely. It should be observed that  $\mathcal{A}_H - (\mathcal{A}_T \cap \mathcal{A}_H) = \mathcal{A}'_H - (\mathcal{A}_T \cap \mathcal{A}'_H)$ .

We found that  $\mathcal{A}'_H \cap \mathcal{A}_T \neq \emptyset$  and the state with  $p_H(\rho_{\text{in}}) > 0.802$  can surely be distilled by the  $T$ -type MSD protocol. Based on this fact, we propose a hybrid protocol, whose flowchart is shown in Fig. 5(a). Got

an ensemble of noisy magic state with the polarization  $p_H(\rho_{\text{in}}) > 0.707$ , we first choose some samples and measure their polarizations in  $T$ -direction to check whether  $p_T(\rho_{\text{in}}) > 0.655$ . If yes, these noisy copies are directly distilled by the five-qubit  $T$ -type MSD module. Otherwise we send them into the four-qubit  $H$ -type MSD module for the higher polarization  $p_H(\rho_{\text{int}})$ .

The distillation protocols require measurements of the code's stabilizers. Only when all measurement outcomes are "0", this round of distillation is successful. Assuming  $\theta$  is the success probability,  $n/\theta$  is the average qubit consumption in each iteration, where  $n = 4, 5, 7$  for the four-qubit, five-qubit and seven-qubit MSD protocols, respectively. Further,  $\nu = \Delta p \theta / n$  is the increased polarization per consumed qubit in each iteration, representing the efficiency of the protocol, where  $\Delta p$  is the increased polarization in the target direction after one iteration. Comparing the efficiency of the four-qubit and five-qubit protocols shown in Fig.5(b), we can see that in the range  $0.707 < p_H < 0.870$ , the four-qubit protocol is more efficient, while beyond this range the five-qubit protocol has higher efficiency. Hence once  $p_H(\rho_{\text{int}})$  reaches the optimal turning point  $p_H^{\text{op}}(\rho_{\text{int}}) = 0.870$ , the intermediate state are then projected to  $T$ -direction by the twirling operation  $D_T$  [10].  $D_T$  converts the polarization from  $H$ -direction to the  $T$ -direction while deducing the polarization by a factor of  $\sqrt{2/3}$ . Next these states are sent into the five-qubit  $T$ -type MSD module for the further distillation. The hybrid protocol ultimately outputs almost pure  $T$ -type magic states. The first criterion ( $p_T(\rho_{\text{in}}) > 0.655$ ) is based on the numerical result that in the region  $\mathcal{A}_T \cap \mathcal{A}_H$ , the five-qubit protocol is less efficient for only 1% of the distillable states. We can see that both ranges  $\mathcal{A}_T$  and  $\mathcal{A}_H$  are distillable by the hybrid protocol. One interesting conclusion is that not just for  $H$ -type magic state, the distillable range for the  $T$ -type magic state is also tight in directions crossing the octahedron edges.

Compared with the seven-qubit MSD protocol, the hybrid protocol can greatly reduce qubit cost for almost all of the distillable region. Figure.5(b) shows that the seven-qubit protocol performs with much lower efficiency in each round of distillation. Not only that, the hybrid protocol has a considerable advantage in the necessary iteration number (Fig.5(c)). For the region  $\mathcal{A}_H - (\mathcal{A}_T \cap \mathcal{A}_H)$  (i.e.,  $p_H(\rho_{\text{in}}) > 0.707$  and  $p_T(\rho_{\text{in}}) < 0.655$ ), the qubit cost can be evaluated as  $(4/\bar{\theta}_4)^{N_4} \cdot (5/\bar{\theta}_5)^{N_5}$  for the hybrid protocol, while  $(7/\bar{\theta}_7)^{N_7}$  for the seven-qubit protocol. Here  $N_{4(5)(7)}$  are the iteration numbers of the 4(5)(7)-qubit MSD scheme and  $\bar{\theta}_{4(5)(7)}$  are the average success probabilities ( $\bar{\theta}_4 = 0.244, \bar{\theta}_5 = 0.124$  and  $\bar{\theta}_7 = 0.046$ ). The hybrid protocol can reduce the qubit cost by a roughly estimated factor of  $10^{35}$  with respect to the seven-qubit MSD protocol [22], with a target polarization above 0.999 (this corresponds to implementing

one non-Clifford operation with theoretical fidelity 0.9995 [23]). The same observation can be extracted for the major part of the region  $\mathcal{A}_T \cap \mathcal{A}_H$  thanks to the property of five-qubit protocol that the increase of the out polarization is exponentially fast in the number of noisy copies when the polarization is high enough [10]. Just for a little region around the pure magic state  $\rho_H$ , the seven-qubit protocol can be slightly more efficient. The exceptional region occupies about 0.57% of the distillable range.

Now we look in detail at the four-qubit  $H$ -type MSD scheme, whose quantum circuit is shown in Fig. 3(a): (i) first prepare four copies of a noisy magic state  $\rho_{\text{in}}^{\otimes 4}$  as the input state; (ii) perform the parity-checking in pairs three times; (iii) if all measurements give 0 result, i.e., the three measured qubits are in the state  $|000\rangle$ , the protocol succeeds and one applies the  $H$ -projection operation  $D_H$  to the qubit that hasn't been measured. The output state is  $\rho_{\text{dis}} \otimes |000\rangle\langle 000|$  with the success probability  $\theta = (2 + 2p_0^2 + p_0^4)/16$ , where  $\rho_{\text{dis}}$  has the output polarization:

$$p_H(\rho_{\text{dis}}) = \frac{6p_0^2 + p_0^4}{\sqrt{2}\{2 + 2p_0^2 + p_0^4\}}. \quad (3)$$

It gives  $p_H(\rho_{\text{dis}}) > p_0$  when  $0.7071 < p_0 < 0.9617$ . Here  $p_0 = p_H(\rho_{\text{in}})$  is the initial polarization of the input states.

We experimentally demonstrate the four-qubit distillation protocol. The physical system is iodotrifluoroethylene ( $\text{C}_2\text{F}_3\text{I}$ ) dissolved in  $d$ -chloroform. One  $^{13}\text{C}$  nucleus and three  $^{19}\text{F}$  nuclei are used as a four-qubit quantum information processor [24, 25]. The natural Hamiltonian of the coupled spin system is  $\mathcal{H} = \sum_i \mathcal{H}_z^i + \sum_{i < j} \mathcal{H}_c^{ij}$ , where  $\mathcal{H}_z^i = \pi v_i \sigma_z^i$  is the Zeeman term,  $v_i$  is the Larmor frequency of spin  $i$ , and  $\mathcal{H}_c^{ij} = (\pi/2) J_{ij} \sigma_z^i \sigma_z^j$  describes the interaction between spin  $i$  and  $j$ ,  $J_{ij}$  is the scalar coupling strength. Experiments were performed on a Bruker AV-500 spectrometer at room temperature. All of the relevant parameters along with the molecular structure are shown in the supplemental material [22].

Figure 3(b) shows the pulse sequence of the experiment, corresponding to the quantum circuit in Fig. 3(a). We first initialized the system in a pseudopure state (PPS) [26]  $\rho_{0000} = (1 - \epsilon)\mathbf{1}/16 + \epsilon|0000\rangle\langle 0000|$  by using line-selective method [22, 25, 27], where  $\epsilon \approx 10^{-5}$  is the polarization. Instead of first four  $H$ -projection operations in Fig. 3(a), four copies of noisy  $H$ -type magic states were prepared by the depolarization procedure shown in the second box of Fig. 3(b). A rotation by an angle  $\gamma$  around the  $y$ -axis transforms  $\sigma_z$  to  $\sigma_z \cos \gamma + \sigma_x \sin \gamma$ . The following gradient field destroys the  $x$  component. By changing the rotation angle  $\gamma$ , we experimentally prepared five sets of noisy magic states, and each set has different average polarization:  $p_H(\rho_{\text{in}}^1) = 0.661, p_H(\rho_{\text{in}}^2) = 0.826, p_H(\rho_{\text{in}}^3) = 0.857, p_H(\rho_{\text{in}}^4) = 0.885, p_H(\rho_{\text{in}}^5) = 0.999$ .

The three parity check gates of Fig. 3(a) were implemented through the distillation procedure in Fig. 3(b).

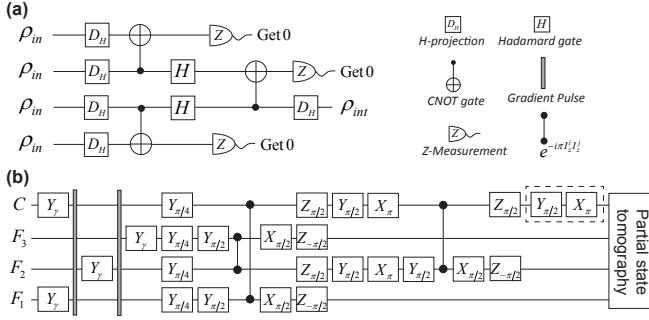


FIG. 3: Quantum circuit (a) and the corresponding pulse sequence (b) for the four-qubit  $H$ -type MSD protocol, where  $X_\alpha = e^{-iaI_x}$ ,  $Y_\alpha = e^{-iaI_y}$  and  $Z_\alpha = e^{-iaI_z}$  denote single-qubit rotations. The  $H$ -projection operation  $D_H(\rho) = (\rho + H\rho H^\dagger)/2$  was realized by accumulating signals of two experiments: one with the Hadamard gate implemented by the pulses shown in the dashed box in (b), and the other without it.

It consists of Clifford operations. At the output side, the  $^{13}\text{C}$  nucleus carries the distilled magic state  $\rho_{\text{dis}}$ . To avoid the error accumulation and exhibit a near-perfect distillation step, we used one high-fidelity shaped pulse gained by the gradient ascent pulse engineering (GRAPE) algorithm [28–30] to implement this sequence. The GRAPE pulses have durations of  $16.8\text{ms}$  with theoretical fidelities above 0.996.

The distilled output state  $\rho_{\text{dis}}$  can be written as (the  $^{13}\text{C}$  nucleus is labeled as qubit 1)

$$\rho_{\text{out}}^{\text{expt}} = \sum_{i=0}^7 \theta_i \rho_i \otimes |i\rangle \langle i| + \sum_{i \neq j=0}^7 \theta_{ij} \rho_{ij} \otimes |i\rangle \langle j|, \quad (4)$$

$$\rho_i = \frac{1}{2} (1 + x_i \sigma_x + z_i \sigma_z),$$

where  $\theta_i$  is the probability of the measurement outcome, corresponding to the resulting state  $|i\rangle$  of the other three redundant qubits, and  $|i\rangle = |000\rangle, |001\rangle, \dots, |111\rangle$ , for  $i = 0, 1, 2, \dots, 7$ . Measuring the outcome  $|000\rangle$  indicates a successful purification. In NMR quantum information processing, since only ensemble measurements are available, we directly measure the expectation value of an observable, without projective measurements. In spite of this, we can obtain all  $\theta_i$ ,  $x_i$  and  $z_i$  using partial quantum state tomography [31] to see the purification effect. Five readout operations are sufficient to determine all the wanted parameters. Firstly, by directly reading the signal of  $^{13}\text{C}$ , we can obtain all  $\theta_i x_i$ ; secondly, by reading the signal of  $^{13}\text{C}$  after the application of a  $\pi/2$  pulse, we can get all  $\theta_i z_i$ ; the additional three readout operations consist of applying a  $\pi/2$  pulse on  $F_1$ ,  $F_2$  and  $F_3$ , then reading the signals. The spectra of the four nuclei after applying a  $\pi/2$  pulse are shown in Fig. 4(a). They are sufficient to determine all diagonal terms of the density matrix, that means we obtain all  $\theta_i = m_{i+1} + m_{i+9}$ ,

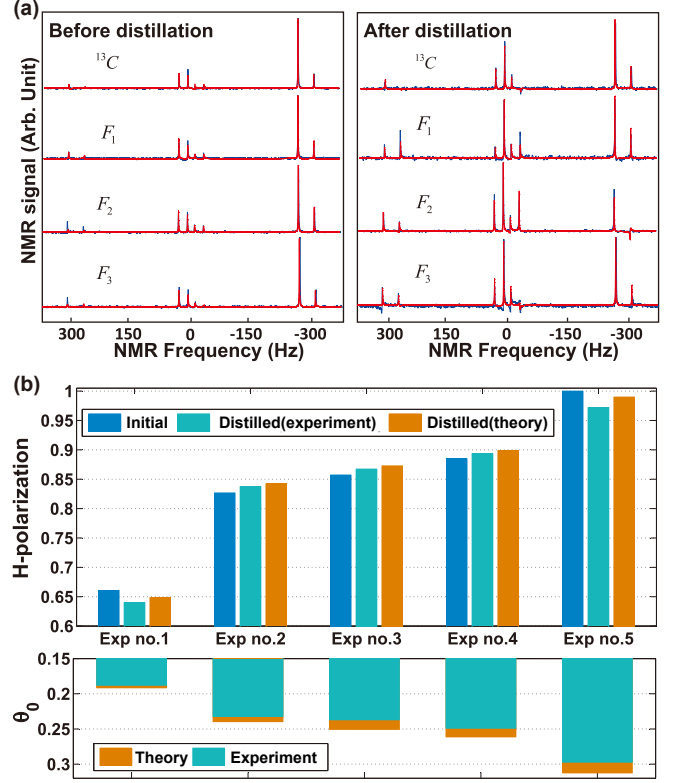


FIG. 4: (a) Experimental results of the distillation. Upper: polarizations along  $H$ -direction before and after distillation. Lower: the success probability  $\theta_0$  of distillation versus to the input polarization. (b) Experimental spectra of the four nuclei before and after distillation for  $p_H(\rho_{\text{in}}) = 0.826$ . The experimentally measured and simulated spectra are shown as the blue and red curves, respectively.

where  $m_i$  represents the  $i$ th diagonal term. Since this sample is unlabeled, we must transfer the polarizations of the  $^{19}\text{F}$  spins to the  $^{13}\text{C}$  spin by SWAP gates and then read the information of the  $^{19}\text{F}$  spin through the  $^{13}\text{C}$  spectrum [32]. The experimental results are shown in Fig. 4(b). The corresponding measured output polarizations are  $p_H(\rho_{\text{out}}^1) = 0.640$ ,  $p_H(\rho_{\text{out}}^2) = 0.838$ ,  $p_H(\rho_{\text{out}}^3) = 0.867$ ,  $p_H(\rho_{\text{out}}^4) = 0.894$ ,  $p_H(\rho_{\text{out}}^5) = 0.979$ . We see that the  $H$ -polarization of the noisy magic states  $\rho_{\text{in}}^2, \rho_{\text{in}}^3, \rho_{\text{in}}^4$  have been experimentally improved by the four-qubit MSD protocol because their input polarizations are in the distillable range. It shows that one can enhance the  $H$ -polarization of the quantum states in  $\mathcal{A}_H$  with initial  $T$ -polarization  $p_T \leq 0.655$  to  $p_H \geq 0.870$  by the four-qubit MSD, and send them into the next step of the hybrid protocol, five-qubit MSD, for converging to the pure magic state  $\rho_T$ .

The total experimental time of the distillation procedure including the readout procedure ranges from  $25\text{ms}$  to  $40\text{ms}$ . It is short compared to the transversal relaxation times of the nuclei (the minimum  $T_2^*$  of the four nuclei is about  $250\text{ms}$ ), so the signal attenuation caused

by the spin-spin relaxation effect is small. We numerically optimized all GRAPE pulses so that they are robust to 5% inhomogeneity of the r.f. field. By doing this, the influence of the r.f. field inhomogeneity is largely eliminated. For the four input copies, the biggest polarization deviation of the individual spin from the average polarization is 0.029. A detailed numerical analysis on the robustness of the distillation algorithm to these differences of input polarizations is presented in the supplemental material [22]. It shows that the distillation algorithm is strongly robust to the imperfect copies of the initial state. The relative deviations between the experimental results and the theoretical expectation are  $0.6\% \sim 1.2\%$ . They mainly come from the imperfections of GRAPE pulses, experimental parameters and data processing.

In conclusion, we presented a hybrid MSD protocol, which aims at taking advantage of different MSD protocols. It further integrates all of the currently known distillable ranges and extends the  $T$ -type distillable range to the stabilizer octahedron edges. Moreover, the hybrid scheme is optimized in efficiency and has a remarkable advantage in saving qubit resources. The hybrid construction exhibits the ability to establish a unified framework for different MSD protocols. It shows that if a state provides quantum computation power in either  $H$ - or  $T$ -direction, it can keep the power in the other magic direction by stabilizer operations. We also experimentally demonstrate the four-qubit scheme by the NMR technology. The present experimental results, together with the previous NMR experiment for the five-qubit protocol, confirm the feasibility of the hybrid MSD scheme. It is expected that as more MSD methods are put forward, more and more distinguished combinations will come out according to the hybrid formalism.

## ACKNOWLEDGMENTS

Y. Yu thanks to get in the topic of "magic state distillation" when she stayed in Laflamme's group. This work is supported by the National Key Basic Research Program of China (Grant No. 2013CB921800), National Natural Science Foundation of China under Grant Nos. 11375167, 11227901, 91021005, the Chinese Academy Of Sciences, the Strategic Priority Research Program (B) of the CAS (Grant No. XDB01030400), Research Fund for the Doctoral Program of Higher Education of China under Grant No. 20113402110044 and the Scientific Research Foundation for the Returned Overseas Chinese Scholars, State Education Ministry.

---

\* These authors contributed equally to this work.

† Electronic address: zhouxy@ustc.edu.cn

- ‡ Electronic address: xhpeng@ustc.edu.cn  
 § Electronic address: djf@ustc.edu.cn
- [1] E. Knill, R. Laflamme, and W. H. Zurek, *Science* **279**, 342 (1998).
  - [2] P. W. Shor, in *Foundations of Computer Science, 1996. Proceedings., 37th Annual Symposium on* (IEEE, 1996) pp. 56-65.
  - [3] A. M. Steane, *Fortschr. Phys.* **46**, 443 (1998).
  - [4] E. Knill, *Nature (London)* **434**, 39 (2005).
  - [5] D. Gottesman, *Phys. Rev. A* **57**, 127 (1998).
  - [6] D. Gottesman, Ph.D. thesis, Caltech, Pasadena, 1997.
  - [7] S. Aaronson and D. Gottesman, *Phys. Rev. A* **70**, 052328 (2004).
  - [8] S. Bravyi, *Phys. Rev. A* **73**, 042313 (2006).
  - [9] M. Howard and J. Vala, *Phys. Rev. A* **85**, 022304 (2012).
  - [10] S. Bravyi and A. Kitaev, *Phys. Rev. A* **71**, 022316 (2005).
  - [11] B. W. Reichardt, *Quantum Inf. Process.* **4**, 251 (2005).
  - [12] E. T. Campbell and D. E. Browne, *Phys. Rev. Lett.* **104**, 030503 (2010).
  - [13] W. van Dam and M. Howard, *Phys. Rev. Lett.* **103**, 170504 (2009).
  - [14] M. Howard, J. Wallman, V. Veitch, and J. Emerson, *Nature* **510**, 351 (2014).
  - [15] N. C. Jones, R. Van Meter, A. G. Fowler, P. L. McMahon, J. Kim, T. D. Ladd, and Y. Yamamoto, *Phys. Rev. X* **2**, 031007 (2012).
  - [16] C. Jones, *Phys. Rev. A* **87**, 042305 (2013); S. Bravyi and J. Haah, *Phys. Rev. A* **86**, 052329 (2012); A. M. Meier, B. Eastin, and E. Knill, *Quant. Inf. Comput.* **13**, 0195 (2013).
  - [17] A. J. Landahl and C. Cesare, arXiv:1302.3240; B. Eastin, *Phys. Rev. A* **87**, 032321 (2013); E. T. Campbell, *Phys. Rev. A* **83**, 032317 (2011).
  - [18] B. W. Reichardt, *Quant. Inf. Comput.* **9**, 1030 (2009).
  - [19] A. M. Souza, J. Zhang, C. A. Ryan, and R. Laflamme, *Nat. Commun.* **2**, 169 (2011).
  - [20] E. T. Campbell and D. E. Browne, in *Theory of Quantum Computation, Communication, and Cryptography*, edited by A. Childs and M. Mosca, *Lecture Notes in Computer Science*, Vol. 5906 (Springer, Berlin/Heidelberg, 2009), pp. 205C32.
  - [21] W. van Dam and M. Howard, *Phys. Rev. A* **83**, 032310 (2011).
  - [22] See Supplemental Material.
  - [23] E. M. Fortunato, M. A. Pravia, N. Boulant, G. Teklemariam, T. F. Havel, and D. G. Cory, *J. Chem. Phys.* **116**, 7599 (2002).
  - [24] X. Peng, J. Zhang, J. Du, and D. Suter, *Phys. Rev. A* **77**, 052107 (2008).
  - [25] X. Peng, Z. Luo, W. Zheng, S. Kou, D. Suter, and J. Du, *Phys. Rev. Lett.* **113**, 080404 (2014).
  - [26] N. A. Gershenfeld and I. L. Chuang, *Science* **275**, 350 (1997).
  - [27] X. Peng, X. Zhu, X. Fang, M. Feng, K. Gao, X. Yang, and M. Liu, *Chem. Phys. Lett.* **340**, 509 (2001).
  - [28] N. Khaneja et al., *J. Magn. Reson.* **172**, 296 (2005).
  - [29] D. Lu, N. Xu, R. Xu, H. Chen, J. Gong, X. Peng, and J. Du, *Phys. Rev. Lett.* **107**, 020501 (2011).
  - [30] N. Xu, J. Zhu, D. Lu, X. Zhou, X. Peng, and J. Du, *Phys. Rev. Lett.* **108**, 130501 (2012).
  - [31] J.-S. Lee, *Phys. Lett. A* **305**, 349 (2002).
  - [32] X. Peng, S. Wu, J. Li, D. Suter, and J. Du, *Phys. Rev. Lett.* **105**, 240405 (2010).

## SUPPLEMENTARY MATERIALS

### 1. The performance of the four-qubit protocol in the asymptotic regime

The iterative function of the four-qubit protocol is

$$\varepsilon_{out} = f(\varepsilon) = 0.5 - \frac{6(1-2\varepsilon)^2 + (1-2\varepsilon)^4}{\sqrt{8} \left[ 2 + 2(1-2\varepsilon)^2 + (1-2\varepsilon)^4 \right]}, \quad (5)$$

where  $\varepsilon = \frac{1-p_H}{2}$  is the error probability. Its first-order Taylor expansion near the polarization  $p_H = 0.962$  (i.e.  $\varepsilon = 0.019$ ) is

$$\begin{aligned} \varepsilon_{out} &= f(0.019) + f'(0.019)(\varepsilon - 0.019) + o[(\varepsilon - 0.019)^2] \\ &= 0.019 + 0.75(\varepsilon - 0.019) + o[(\varepsilon - 0.019)^2]. \end{aligned} \quad (6)$$

$\varepsilon^* = 0.019$  is the convergence value, and the convergence rate is linear, which is different from the five-qubit protocol's quadratic convergence in the asymptotic regime. For the input  $\varepsilon_0$ , after the first iteration,  $\varepsilon_1 \approx 0.019 + 0.75(\varepsilon_0 - 0.019)$ . After the second iteration,  $\varepsilon_2 \approx 0.019 + 0.75^2(\varepsilon_0 - 0.019)$ . After  $k$  times of iterations,  $\varepsilon_n \approx 0.019 + 0.75^k(\varepsilon_0 - 0.019)$ . Near the  $p_H = 0.962$ , we can approximate the success probability  $\theta_s \approx \theta(0.962) = 0.294$ . The total number of initial noisy magic states  $N = (4/\theta_s)^n \approx (13.6)^k$ . So

$$\begin{aligned} \varepsilon_{out} &\approx 0.019 + 0.75^{\log_{13.6} N} (\varepsilon_0 - 0.019) \\ &= 0.019 + N^{\left(\frac{1}{\log_{0.75} 13.6}\right)} (\varepsilon_0 - 0.019). \end{aligned} \quad (7)$$

The error rate in the distilled magic states is reduced polynomially with respect to the number of noisy input magic states.

Nevertheless, in our hybrid scheme, before the polarization reaches the asymptotic regime of the four-qubit protocol, we switch to the five-qubit protocol which gives an exponential decay of the error rate. The four-qubit protocol shows the ability of reducing the qubit cost mainly rooted in its less qubit cost in every round of distillation, which brings about the higher efficiency than five-qubit protocol before the optimal turning point ( $p_H = 0.870$ ).

### 2. The integration between the 4-qubit $H$ -type MSD and the 5-qubit $T$ -type MSD

In the hybrid magic state distillation (MSD) scheme, the noisy copies firstly enter into  $H$ -type MSD modules as four qubits in one group. With the increase of iterations number, the modules output states more closer to  $H$ -type magic state. Certainly, their polarizations of  $T$ -direction

$p_T$  also increase. Once  $p_H$  is higher than the optimal turning point ( $p_H = 0.87$ , corresponding to  $p_T = 0.71$ ), the state enters into  $T$ -type MSD module. Then after several iterations of  $T$ -type MSD, we obtain states with  $p_T \sim 1$ . Fig. 5 shows the integration between the two schemes.

### 3. The qubit cost in the low polarization range $\mathcal{A}_H - (\mathcal{A}_T \cap \mathcal{A}_H)$

From Fig. 6, we can obtain the average success probability for one iteration ( $\bar{\theta}_4 = 0.244$ ,  $\bar{\theta}_5 = 0.124$  and  $\bar{\theta}_7 = 0.046$ ). For the region  $\mathcal{A}_H - (\mathcal{A}_T \cap \mathcal{A}_H)$ , the necessary iteration number to achieve a  $T$ -type or  $H$ -type magic state with a target polarization above 0.999 is about 26 using the seven-qubit protocol. The qubit cost is evaluated as  $(7/\bar{\theta}_7)^{26} \sim 10^{56}$ . Using the hybrid protocol, it needs about 11 iterations of the four-qubit protocol and 5 iterations of the five-qubit protocol. The qubit cost is evaluated as  $(4/\bar{\theta}_4)^{11} \cdot (5/\bar{\theta}_5)^5 \sim 10^{21}$ . Hence the qubit cost is reduced by a factor of about  $10^{35}$  using the hybrid protocol for the low polarization range  $\mathcal{A}_H - (\mathcal{A}_T \cap \mathcal{A}_H)$ .

As an example, table I shows the performance of the hybrid protocol and the 7-qubit protocol, when they are used to distill one noisy state whose polarization is in  $H$ -direction ( $p_H = 0.78$ , equivalent to  $p_T = 0.636$ ). Though the target states of the two schemes are different ( $p_H = 0.99$  in the 7-qubit case,  $p_T = 0.999$  in the hybrid case), either of the target states can be used to implement one non-Clifford operation with theoretical fidelity 0.9995. We can see that the hybrid protocol requires less iterations and possesses much higher successful probability than the 7-qubit protocol, which lead to the great saving in qubit cost.

### 4. The efficiency of the whole procedure

The parameter  $\nu = \Delta p_{T(H)} \theta / n$  represents the increased polarization per consumed qubit in each iteration. The hybrid protocol is optimized by  $\nu$ . The efficiency of the whole procedure of  $k$  times distillation is defined as

$$V = \frac{\Delta p_1 + \Delta p_2 + \cdots + \Delta p_k}{n_1 n_2 \cdots n_k / \theta_1 \theta_2 \cdots \theta_k}. \quad (8)$$

Both  $\nu$  and  $V$  is determined by two parameters: increment  $\Delta p_{T(H)}$  gained from one iteration and the average qubit consumption  $n/\theta$  in one iteration. Given a target polarization, the optimal turning point may be slightly different from the one calculated by the efficiency  $\nu$ . Setting the target  $P_T = 0.999$ , for different initial polarizations, we numerically calculated the optimal turning points, which are shown in Fig. 7. We can see the optimal turning points gather around  $p_H = 0.85$ , which

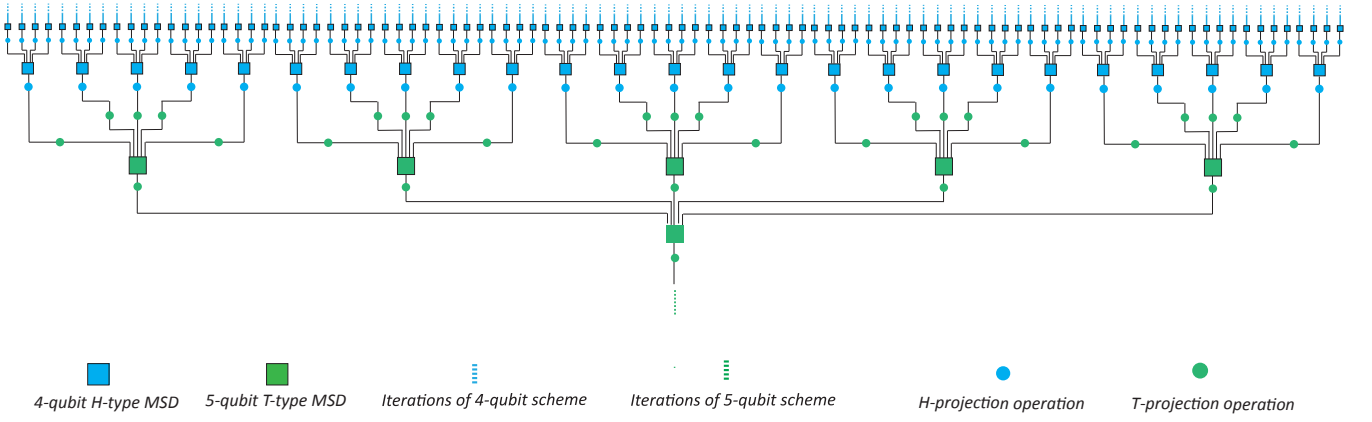


FIG. 5: The integration between the 4-qubit  $H$ -type MSD and the 5-qubit  $T$ -type MSD.

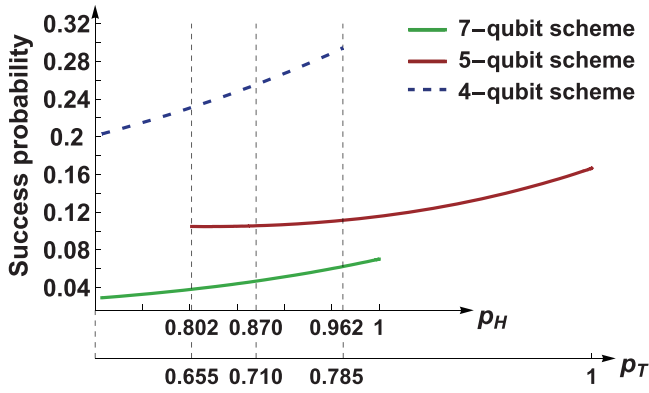


FIG. 6: The success probability of the three individual MSD protocols.

is slightly different from the hybrid protocol's turning points  $p_H = 0.87$ .

### 5. The hybrid protocol

Once the polarization reaches the turning point  $p_H = 0.87$  of the hybrid protocol, the  $T$ -projection operation  $D_T$  is performed to the state. Then we get a polarization of  $T$ -direction with  $P_T > 0.71$ .

1. If  $p_T(\rho_{in}) > 0.71$ , we directly distill them with five-qubit protocol.
2. If  $0.655 < p_T(\rho_{in}) < 0.71$  and  $p_H(\rho_{in}) < 0.707$ , the state can't benefit from the four-qubit protocol. We should distill it with the five-qubit protocol.
3. If  $p_T(\rho_{in}) < 0.655$  and  $0.707 < p_H(\rho_{in})$ , the state can't directly benefit from the five-qubit protocol. We should firstly distill it to  $p_H(\rho_{in}) = 0.87$  with the four-qubit protocol.
4. If  $0.655 < p_T(\rho_{in}) < 0.71$  and  $0.707 < p_H(\rho_{in}) < 0.87$ , for about 95% of the states in this range, it's better to directly distill them with the five-qubit protocol.

Iteration	Output polarization		Successful probability		Qubit cost	
	7-qubit scheme( $p_H$ )	Hybrid scheme( $p_T$ )	7-qubit scheme	Hybrid scheme	7-qubit scheme	Hybrid scheme
1	0.8001	0.6471	0.0359	0.2242	195	17.84
2	0.8226	0.6584	0.0380	0.2282	3592	312
3	0.8465	0.6706	0.0407	0.2327	$10^6$	5376
4	0.8703	0.6833	0.0437	0.2377	$10^8$	$10^4$
5	0.8928	0.6962	0.0470	0.2432	$10^{11}$	$10^6$
6	0.9129	0.7090	0.0504	0.2489	$10^{13}$	$10^7$
7	0.9301	0.7213	0.0536	0.2548	$10^{15}$	$10^8$
8	0.9445	0.7723	0.0566	0.0907	$10^{17}$	$10^{10}$
9	0.9562	0.8490	0.0613	0.0996	$10^{19}$	$10^{12}$
10	0.9656	0.9356	0.0632	0.1166	$10^{21}$	$10^{13}$
11	0.9730	0.9890	0.0646	0.1423	$10^{23}$	$10^{15}$
12	0.9789	0.9997	0.0658	0.1622	$10^{25}$	$10^{16}$
13	0.9835		0.0668		$10^{27}$	
14	0.9872		0.0676		$10^{29}$	
15	0.9900		0.0682		$10^{31}$	
16	0.9922		0.0686		$10^{33}$	
17	0.9939		0.0690		$10^{35}$	
18	0.9953		0.0693		$10^{37}$	
19	0.9963		0.0695		$10^{39}$	
20	0.9971		0.0697		$10^{41}$	
21	0.9978		0.0698		$10^{43}$	
22	0.9983		0.0699		$10^{45}$	
23	0.9987		0.0700		$10^{47}$	
24	0.9990		0.0701		$10^{49}$	

TABLE I: Comparing the performance of the hybrid MSD protocol and the 7-qubit protocol, when they are used to distill one noisy state of  $H$ -direction with  $p_H = 0.78$ . Since the target direction of the hybrid protocol is  $T$ -direction, the polarizations gained by the subprocedure of the 4-qubit  $H$ -type protocol have been converted to  $T$ -direction, i.e., multiplied by the factor  $\sqrt{2/3}$ .

### 6. Robustness of the 4-qubit $H$ -type MSD algorithm

In the theoretical analysis, the input of the 4-qubit  $H$ -type MSD algorithm is four qubits with the same polarization of  $H$ -direction. However, it is impossible to prepare each qubit to totally identical state. It is unavoidable that there are some differences between the



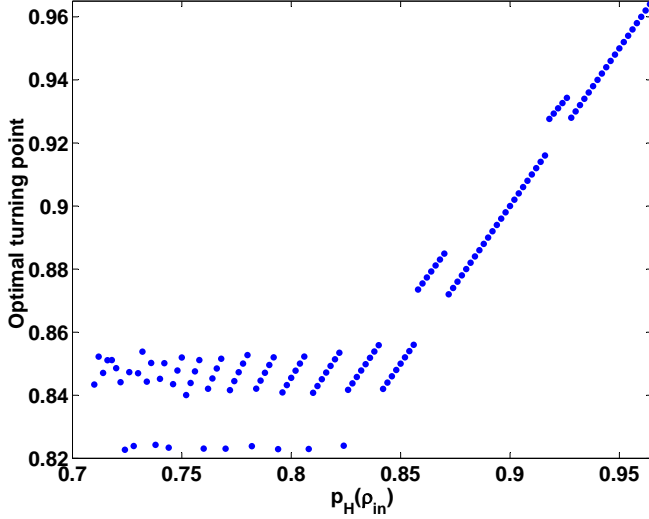


FIG. 7: The optimal turning points for different input polarizations with the target polarization above 0.999. The optimal turning points gather around  $p_H = 0.85$ . If the input state's polarization is higher than 0.86, it's better to distill them directly using the five-qubit  $T$ -type MSD protocol.

polarizations of the four copies in the experiment. Table. II shows the initial polarizations in our experiment. We can see that the biggest polarization deviation of the individual spin from the average polarization is 0.029. It is important to analyze the robustness of the distillation algorithm to these differences of polarizations of input states.

Figure. 8a shows the average distillation effect versus to both the input polarization and the deviation. For every centre point which range from 0.68 to 0.99, we choose the deviations from 0 to 0.3. For each deviation, we randomly choose 100 inputs, then calculate the value  $p_{out} - p_{in}$  for each input. We use the average of  $p_{out} - p_{in}$  to evaluate the purity effect of the algorithm at this centre point. It shows that this distillation algorithm is strongly robust to the differences of polarization between the input qubits. Figure. 8b shows the output polarization corresponding to gaussian distribution input. We can see the distributions of output present larger average and smaller variance comparing to input distribution.

## 7. Sample information

The physical system we used is the molecules of Iodotrifluoroethylene ( $C_2F_3I$ ) dissolved in d-chloroform. As  $^{13}C$  and  $^{19}F$  are spin- $\frac{1}{2}$  nuclei, four qubits can be encoded using this sample for NMR quantum information processing. The natural Hamiltonian of the coupled spin system is,  $\mathcal{H} = \sum_i \mathcal{H}_i^z + \sum_{i < j} \mathcal{H}_{ij}^c$ , where  $\mathcal{H}_i^z = \pi \nu_i \sigma_z^i$  is the Zeeman Hamiltonian,  $\nu_i$  is the Larmor frequency of

nuclear spin	H-polarization of Initial state	Average polarization of Initial state
C	0.6436	0.6607
F1	0.6602	
F2	0.6719	
F3	0.6667	
nuclear spin	H-polarization of Initial state	Average polarization of Initial state
C	0.8135	0.8266
F1	0.8330	
F2	0.8444	
F3	0.8152	
nuclear spin	H-polarization of Initial state	Average polarization of Initial state
C	0.8476	0.8572
F1	0.8538	
F2	0.8591	
F3	0.8664	
nuclear spin	H-polarization of Initial state	Average polarization of Initial state
C	0.8603	0.8849
F1	0.9016	
F2	0.9138	
F3	0.8632	
nuclear spin	H-polarization of Initial state	Average polarization of Initial state
C	0.9927	0.9998
F1	1.0009	
F2	1.0077	
F3	0.9984	

TABLE II: The polarizations of the prepared initial states.

spin  $i$ , and  $\mathcal{H}_{ij}^c = (\pi/2) J_{ij} \sigma_z^i \sigma_z^j$  describes the interaction between spin  $i$  and  $j$ ,  $J_{ij}$  is the scalar coupling strength. All of the relevant parameters along with molecular structure are shown in Fig. 9.

## 8. PPS preparation

The system is originally in the thermal equilibrium state  $\rho_{eq} = I/16 + \sum_{i=1}^4 \varepsilon_i I_z^i$ , where  $\varepsilon_i \sim 10^{-5}$  and  $I = (I_x, I_y, I_z)$  is the spin vector operator. For PPS  $\rho_{0000} = (1 - \varepsilon)I/16 + \varepsilon|0000\rangle\langle 0000|$ , the populations of all energy levels must be equalized except the first level. For this purpose, we numerically found an array  $\{x_\alpha\}_{\alpha=1,\dots,14}$ , which determines a unitary operator

$$U_1 = \sum_{\alpha} \exp \left[ -ix_{\alpha} I_x^{(\alpha+1, \alpha+2)} \right], \quad (9)$$

$I_x^{(\alpha+1, \alpha+2)}$  is the single quantum transition operator between levels  $\alpha + 1$  and  $\alpha + 2$ . The  $U_1$  satisfies following requirement:  $\text{diag}[U_1 \rho_{eq} U_1^\dagger] = \text{diag}[\rho_{0000}]$ . That is, this unitary operator achieves saturation of latter 15 energy levels, while the population of the first level keeps unchanged. Then one gradient field pulse destroys all the coherences except homonuclear zero coherences of  $^{19}F$



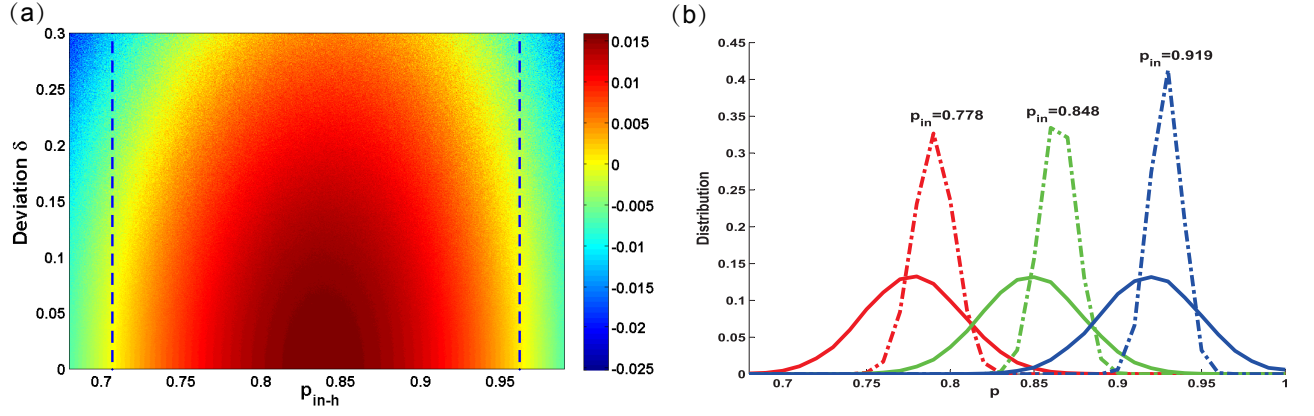


FIG. 8: (a) Distillation effect versus to average input polarization and the deviations of input polarizations from the average value. For example, the point (0.82, 0.08) in the  $\delta$  &  $p_{in}$  plane, means that we randomly choose the input polarizations from the range 0.82-0.08 to 0.82+0.08. The blue perpendicular lines represent the theoretical distillable boundary. (b) Distributions of output polarization correspond to gaussian distribution inputs. The solid curves represent the input polarization of gaussian distributions with centre at 0.778, 0.848 and 0.919. The dashed curves show the distributions of output.

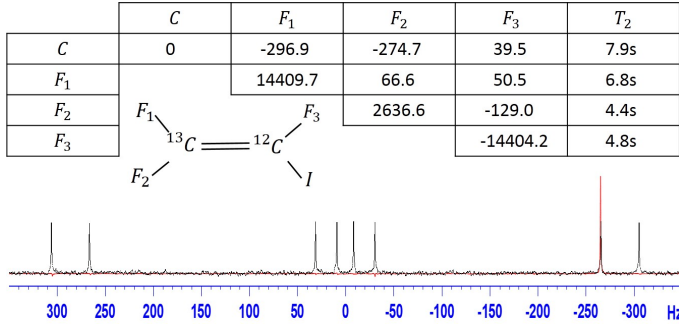


FIG. 9: Characteristics of the four-qubit quantum register. The inset shows the structure, where the four qubits are labeled as  $^{13}C$ ,  $F_1$ ,  $F_2$ ,  $F_3$ . The chemical shifts and scalar coupling constants (in Hz) are on and above the diagonal in the table, respectively. The last column shows the transversal relaxation time  $T_2$  of each nucleus measured by CPMG sequences. Shown below are spectra of  $^{13}C$  obtained by  $\pi/2$  readout pulses when the system is prepared in the thermal equilibrium state (black) and PPS  $\rho_{0000}$  (red).

nuclei. The other specially designed unitary operator  $U_2$  applies to the system, which transforms these redundant zero coherences to others that can be eliminated by gradient field pulse. Then applying another gradient field pulse, we prepare the PPS  $\rho_{0000}$ . As  $U_1$  is obtained by numerical search and  $U_2$  is actually a combination of some CNOT gates between two selected levels, it is hard to find out a conventional pulse sequence to implement these two unitary operators. We engineered each operator as an individual shaped pulse by the gradient ascent pulse engineering (GRAPE) algorithm [28]. These two GRAPE pulses are of the duration around 25ms with the theoretical fidelity above 0.994 and they are also designed with robustness against the rf inhomogeneity.

## 9. Experimental results of 4-qubit H-type MSD

Table III shows the experimental results 4-qubit H-type MSD. The middle three inputs are in the distillable range. We observe higher polarizations corresponding to these three inputs.

Initial polarization	Polarization after distillation	Success probability
0.661	0.640	0.188
0.827	0.838	0.232
0.857	0.867	0.237
0.884	0.894	0.249
0.999(8)	0.979	0.297

TABLE III: Experimental results of 4-qubit H-type MSD.

## 10. State tomography

### Input state tomography

The input state can be written as

$$\begin{aligned} \rho_0 &= \frac{1}{2} [I + x_1(\sigma_x + \sigma_z)] \otimes \frac{1}{2} [I + x_2(\sigma_x + \sigma_z)] \otimes \dots \\ &\quad \frac{1}{2} [I + x_3(\sigma_x + \sigma_z)] \otimes \frac{1}{2} [I + x_4(\sigma_x + \sigma_z)] \\ &= \sum_{i=0}^7 \sum_{j=0}^7 \frac{1}{2} [I + x_1(\sigma_x + \sigma_z)] \otimes m_{ij} |i\rangle \langle j|, \end{aligned}$$

where  $\sum_{k=0}^7 m_{kk} = 1$ ,  $|i(j)\rangle = |000\rangle, |001\rangle, \dots, |111\rangle$ . So we can get  $x_1$  by summing all signals of qubit 1. Similarly, we can get all  $x_i$ . The average of  $x_i$  is viewed as the polarization  $x_{in}$  of input state.

*Distilled state tomography*

The state after distillation can be written as (assuming qubit 1 carries the distilled magic state)

$$\rho_{out}^{exp} = \sum_{i=0}^7 \theta_i \rho_i \otimes |i\rangle \langle i| + \sum_{i \neq j=0}^7 \theta_{ij} \rho_{ij} \otimes |i\rangle \langle j|,$$

$$\rho_i = \frac{1}{2} (I + x_i \sigma_x + z_i \sigma_z),$$

where  $\theta_i$  is the probability of the measurement outcome, corresponding to the resulting state  $|i\rangle$  of the other three redundant qubits, and  $|i\rangle = |000\rangle, |001\rangle, \dots, |111\rangle$ , for  $i = 0, 1, 2, \dots, 7$ . Measuring outcome  $|000\rangle$  indicates a successful purification. We can determine all the wanted

parameters by following steps:

**a.** Read out on each qubit after the application of a  $\pi/2$  pulse;

By this step, we can get all diagonal elements  $\{m_i\}_{i=1, \dots, 16}$  of  $\rho_{out}^{exp}$ .

For example, after operating a  $\pi/2$  pulse on qubit 1, the intensity of the spectral line, which corresponds to the transition  $|0000\rangle$  to  $|1000\rangle$ , is proportional to the difference between the corresponding populations, i.e.  $m_1 - m_9$ .

Then we get all  $\theta_i = m_i + m_{i+8}$ .

**b.** Read out on qubit 1 and read out on qubit 1 after the application of a  $\pi/2$  pulse; These two readout operations are sufficient to measure all  $\theta_i \rho_i$ .